



TITLE:

Analysis of structures of rubber-filler systems with combined scattering methods

AUTHOR(S):

Takenaka, Mikihiro

CITATION:

Takenaka, Mikihiro. Analysis of structures of rubber-filler systems with combined scattering methods. Polymer Journal 2013, 45(1): 10-19

ISSUE DATE:

2013-01

URL:

<http://hdl.handle.net/2433/177005>

RIGHT:

© 2013 The Society of Polymer Science, Japan.; This is not the published version. Please cite only the published version.; この論文は出版社版ではありません。引用の際には出版社版をご確認ご利用ください。

Analysis of Structures of Rubber-Filler Systems
with Combined Scattering Methods

Mikihito Takenaka^{1,2}

¹Department of Polymer Chemistry, Graduate School of Engineering,

Kyoto University, Kyoto 615-8510, JAPAN

²Structural Materials Science Laboratory, SPring-8 Center, RIKEN Harima Institute

Research, 1-1-1, Kouto, Sayo-cho, Sayo-gun, Hyogo 679-5198, JAPAN

Correspondence: Mikihito Takenaka, Department of Polymer Chemistry, Graduate
School of Engineering, Kyoto University, Kyoto 615-8510, JAPAN

E-mail: takenaka@alloy.polym.kyoto-u.ac.jp

Running Head: Scattering Studies of Rubber-Filler Systems

Abstract

This review presents an analysis of the hierarchical structures formed in rubber-filler systems by using combined scattering methods. The combined scattering methods utilize various scattering methods and are powerful tools for the quantitative characterization of hierarchical structures over a wide range of length scales, ranging from nanometers to micrometers. Scattering theories for the analysis of the experimental scattering functions and their applications are described.

Keywords: combined scattering methods/ hierarchical structure/ rubber-filler systems

INTRODUCTION

Rubber-filler systems have been widely used in industrial applications, such as for tires and belts so on¹⁻⁶. The use of fillers in rubber compounds reinforces the rubber material and improves the barrier properties. There are several important factors for controlling the efficiency of rubber reinforcement by fillers. The dispersion of filler particles in the rubber matrix is one of the most important factors in this process. Typically, following the use of conventional compounding processes, the fillers are not dispersed homogeneously and form hierarchical structures within the rubber matrices. For example, in rubber-carbon black (CB) systems, the CB primary particles are not distributed independently but coalesce into aggregates, which are indestructible units of CB, during conventional compounding processes². The aggregates of CB, which are called aggregates or agglomerates, can also lead to the formation of hierarchical structures which consist of higher levels of ordered structure². It is believed that the hierarchical structures affect the efficiency of filler reinforcement. Other rubber-filler systems also form hierarchical structures; furthermore, the characteristic lengths and morphologies of each level of ordered structure, such as agglomerates, vary with the specific combination of rubber and filler used in the system in addition to the compounding processes. To analyze the hierarchical structure, scattering techniques are one of useful techniques. In scattering experiments, we investigated the angular dependence of the scattered intensities induced by the incident beam hitting samples. Although the interpretation of the scattering intensities is complicated, nonetheless, scattering techniques are suitable for obtaining the statistical features of rubber-filler

systems. However, the length scales of the hierarchical structures can extend from nanometers to micrometers, which prevents the characterization of hierarchical structures with a single scattering method. In particular, we cannot evaluate the quantitative features, such as the size and morphology of each level, from the scattering intensity obtained by a single scattering method because we cannot eliminate the possible effects of higher and lower levels of the hierarchical structure on the scattering intensity when limited to a region of small q values.

In this review, I focus on the structural analysis of rubber-filler systems by using combined scattering methods. The combined scattering approaches utilize various individual scattering methods, including wide-angle scattering, small-angle scattering, and ultra-small-angle scattering with X-ray and neutron beams. In combination, the methods are powerful tools for the quantitative characterization of rubber-filler hierarchical structures over a wide range of length scales (from the nanometer to the micrometer scale). Thus, we can employ these combined methods to extract useful information regarding the hierarchical structures of rubber-filler systems. Moreover, combined scattering methods enable us to investigate hierarchical structures under various sample environments, such as extension or shear deformation. We can expect to identify correlations between the mechanical properties and the respective structures during deformation processes by using combined scattering methods.

In the next section, we summarize the features of the various scattering techniques used in combined scattering methods and present the details of ultra-small-angle

scattering instruments using X-ray and neutron beams. Then, the model expressions to analyze the experimentally obtained scattering functions are described. In the subsequent section, the experimental results of the rubber-filler system scattering data are presented. Finally, we conclude the review.

VARIOUS SCATTERING METHODS

Figure 1 shows the wavenumbers (q -regions) or length scales that can be observed with various scattering techniques and the associated hierarchical structures of the rubber-filler systems. Here, q is defined by

$$q = \frac{4\pi}{\lambda} \sin \frac{\theta}{2} \quad (1)$$

with λ and θ defined as, respectively, the wavelength of the incident beam and the scattering angle in the medium. The length scale Λ is expressed by $\Lambda = 2\pi/q$. The various scattering methods are summarized in subsequent sections. Before describing the method, we must mention the q -region of each scattering method. The q regions covered by each scattering method are described in the subsequent parts of this section. It should be noted that the region varies with the specific experimental conditions, such as the path length, the wavelength of the incident beam, and the detector resolution.

X-ray scattering

Scattering methods with X-ray incident beams include wide-angle X-ray scattering or diffraction (WAXS or XRD), small-angle X-ray scattering (SAXS), and ultra-small-angle X-ray scattering (USAXS). The scattering of X-rays is induced by fluctuations in the electron density, and the scattering power increases with atomic number⁷.

WAXS or XRD techniques span the range of $7 < q < 30 \text{ nm}^{-1}$ and are widely used in the analysis of crystalline structures. For rubber-filler systems, we can observe the amorphous peaks of the rubber and the filler as well as the crystalline structure of the rubber induced by strain⁸⁻¹⁰.

The q region observed with SAXS is at $0.05 < q < 7 \text{ nm}^{-1}$. Larger q -regions, such as $7 < q < 4 \text{ nm}^{-1}$, in SAXS are dominated by thermal diffusion scattering (TDS), which originates in the density fluctuations within rubbers and is related to the free volume of the amorphous region. In smaller q regions in SAXS, we can observe the structures of the filler aggregates, such as the interfacial structure between the rubber and the fillers, the size and distributions of the primary filler particles, and the size of the aggregates as well as their internal structures. It should be noted that scattering from the interfacial region can not avoid the effects of TDS; hence we must evaluate the TDS with the method given by Ruland¹¹ and Vonk¹². This method requires that we subtract the TDS from the scattering intensity before evaluating any interfacial structures, such as the interfacial thickness^{13,14}. The specifics of the SAXS and USAXS analytical techniques are described later with respect to their application to aggregates.

We can observe smaller q regions, such as the range of $0.001 < q < 0.05 \text{ nm}^{-1}$, by

using USAXS because this range is not accessible with SAXS. Thus, USAXS is useful for investigating agglomerates and the dispersion of filler aggregates in rubber.

Neutron scattering

For structural analyses of rubber-filler systems, small-angle neutron scattering (SANS) and ultra-small-angle neutron scattering (USANS) are widely used neutron scattering methods. Rubber–filler systems contain significant quantities of H atoms, which make it difficult to analyze the scattering at $q > 1.0 \text{ nm}^{-1}$ because incoherent scattering becomes dominant in this q region. Unlike X-ray scattering, neutron scattering power is independent of atomic number because neutrons interact only with atomic nuclei¹⁵. As for typical rubber-filler systems, such as natural rubber/ carbon black and poly(styrene-*ran*-butadiene)/ silica, there exists a significant degree of contrast between the phases to allow for the collection of scattering function measurements. Thus, it is not necessary to synthesize deuterated polymers for neutron scattering to be able to analyze the structures of the aggregates of fillers.

SANS covers $0.01 < q < 1 \text{ nm}^{-1}$, which is similar to the q region covered by SAXS. SANS reflects the structure of the filler aggregations in addition to SAXS. We can observe the scattering intensity at $2 \times 10^{-4} < q < 0.01 \text{ nm}^{-1}$ with USANS. The q region accessed by USANS reflects the agglomerate morphologies and the filler aggregate dispersions within the rubber.

Although many good reviews and books on the SAXS and SANS techniques have been published⁷, there are few reviews of USAXS and USANS. Thus, we provide a

brief review of USAXS and USANS in the next section.

ULTRA-SMALL-ANGLE SCATTERING

Ultra-Small-Angle X-ray Scattering

According to the definition of q (eq. (1)), we must measure the angular dependence of the scattered intensity with high angular resolution in the small angle region due to the inherently short wavelengths of X-rays, such as $\lambda=0.154$ nm for Cu-K α . To attain such a small q region (on the order of 10^{-3} nm $^{-1}$), two techniques are available: the Bonse-Hart camera and the long path camera, which is used with synchrotron radiation X-rays.

The Bonse-Hart camera for X-ray scattering

The camera was originally invented by Bonse-Hart¹⁶. Figure 2 presents a schematic picture of the USAXS instrumentation¹⁷. The USAXS optics consist of the monochromator and the analyzer, both of which are fabricated from either silicon or germanium. The sample is placed between the monochromator and the analyzer. The monochromator collimates the incident X-ray source. The q -dependence of the scattered intensity is measured by rocking the analyzer, which allows the desired high q resolution to be attained. We can achieve the minimum q ($q_{\min} \cong 1.0 \times 10^{-3}$ nm $^{-1}$) when using the Bonse-Hart camera in X-ray scattering experiments. The advantage of the Bonse-Hart camera is that conventional X-ray sources can be utilized (such as rotating anode X-ray generator) as the incident beam. However, the measured intensity is significantly affected by the smearing effects, which are caused by the incident beam

profile. Thus, the use of a desmearing procedure is necessary to obtain the true scattering profile. Ultimately, based on this approach, the sample should be isotropic. Moreover, the scattered intensity is detected stepwise, which indicates that we can not follow rapid changes in structure with the Bonse-Hart camera. Recently, Bonse-Hart cameras have also been installed at synchrotron facilities^{18,19}. In particular, Ilavsky et al. succeeded in measuring two-dimensional USAXS images by using two sets of monochromators and analyzers, which were positioned both vertically and horizontally²⁰.

Long path camera with synchrotron radiation X-ray

To attain increased angular resolution, we also can use a long sample-to-detector distance. The advantage of using the long sample-to-detector is that its use affords us the ability to measure 2D USAXS patterns, which can not be obtained with the Bonse-Hart camera. Figure 3 shows a schematic drawing of the USAXS setup at BL20XU, SPring-8, Japan^{21,22}. The path length at BL20XU is set to be 160 m; with this length, the q -range $1.5 \times 10^{-3} < q < 2.5 \times 10^{-2} \text{ nm}^{-1}$ can be obtained with an X-ray energy of 23 keV. For rubber-filler systems, we can collect the scattered images in 2 sec intervals by using a CCD detector coupled with an X-ray image intensifier, which allows in situ measurements to be carried out under deformation. USAXS measurements also can be obtained at BL19B2, SPring-8, Japan²³. The path length at BL19B2 is approximately 40 m, and the corresponding q -range is $3.0 \times 10^{-3} < q < 1.0 \times 10^{-1} \text{ nm}^{-1}$ with an X-ray energy of 18 keV. BL19B2 is a bending magnet beamline, which means that the scattered intensity of this beamline is weaker than that measured

at the BL20XU undulation beamline. However, the high q region at BL19B2 significantly overlaps with the typical SAXS region such that we can easily combine the USAXS patterns with SAXS patterns.

Ultra-Small-Angle Neutron Scattering

Bonse-Hart camera for neutron scattering

Bonse-Hart cameras for neutron scattering experiments are also available at neutron facilities²⁴⁻²⁷. Silicon single crystals are used as the monochromators and the analyzers in this technique as well as in the USAXS instruments. Bonse-Hart cameras used in neutron scattering experiments can cover $2 \times 10^{-4} < q < 4 \times 10^{-3} \text{ nm}^{-1}$ with an incident neutron wavelength of 0.2 nm. The value of $q_{\min} \cong 2 \times 10^{-4} \text{ nm}^{-1}$ for the Bonse-Hart camera in USANS is smaller than that of the Bonse-Hart camera in USAXS ($q_{\min} \cong 1.0 \times 10^{-3} \text{ nm}^{-1}$). This difference originates in the respective differences in the half-width at half-maximum values of the Bragg reflections ($\Delta\theta$) in neutron scattering and X-ray scattering; that is, $\Delta\theta$ limits the q_{\min} . According to the dynamical theory of diffraction, $\Delta\theta$ is described by²⁶

$$Dq = \frac{b_c e^{-w} |F|^2}{\rho V_c \sin(2q_B)} \quad (2)$$

where b_c , e^{-w} , F , λ , θ_B , and V_c are, respectively, the coherent scattering length, the Debye-Waller factor, the structure factor of the crystal, the wavelength of the incident

beam, the Bragg angle, and the volume of unit crystal. For Si, b_c of neutron is significantly smaller than that of the X-ray; therefore, we can attain a smaller q by using neutron.

Focusing SANS

The use of focusing collimators (biconcave MgF_2 lenses) enables us to measure a lower q region than that accessible by pinhole SANS²⁸. Figure 4 shows a schematic picture of focusing SANS at SANS-J-II, JRR-3, Japan^{29,30}. A high-resolution area detector with 0.5 mm positional resolution was installed in addition to a MgF_2 lens resulting in a value of $q_{\min} \cong 3 \times 10^{-3} \text{ nm}^{-1}$ is attained; in contrast, the q_{\min} of pinhole SANS is $3 \times 10^{-3} \text{ nm}^{-1}$. Although the q_{\min} of focusing SANS is larger than that of USANS, we can obtain 2D scattering patterns and measure anisotropic structures, such as the scattering pattern of rubber-filler systems under extension. Focusing SANS is also available at SANS-U, JRR-3, Japan³¹ and several neutron facilities³²⁻³⁴.

Notably, the smearing effects also affect the scattering function obtained by use of the long path camera with synchrotron radiation X-ray and focusing SANS even though the effects are weaker than those for the Bonse-Hart camera.

SCATTERING THEORY FOR RUBBER-FILLER SYSTEMS

The unified Guinier/power-law

As described previously, rubber-filler systems form hierarchical structures. By combining the various scattering methods described in the previous section, we can obtain the scattering profiles over five decades in q scale. To describe the scattering

profiles of the rubber-filler systems over five decades, Beuacage proposed a unified Guinier/power-law method^{35,36}. According to this method, the hierarchical structure with an arbitrary number n of hierarchical levels can be described by

$$I(q) = \sum_{i=1}^n \left\{ G_i \exp\left(\frac{-q^2 R_{g,i}^2}{3}\right) + B_i \exp\left(\frac{-q^2 R_{g,i+1}^2}{3}\right) \left[\frac{\left(\operatorname{erf}\left(q R_{g,i} / \sqrt{6}\right)\right)^3}{q} \right]^{P_i} \right\} \quad (3)$$

where G_i , B_i , and P_i are, respectively, the Guinier prefactor of the i -th level structure with a radius of gyration $R_{g,i}$, a prefactor of the power-law scattering of the i -th level structure, and the exponent of the power-law scattering, which characterizes the shape of the i -th level structure. $i = 1$ refers to the largest-size structural level. If the structure has a sharp interface, the scattering is proportional to q^{-4} or $P_i = 4$ and $B_i = 2\pi\Delta a^2 S$, where S is the surface area of the i -th level structure and Δa is the electron density or the scattering length density of the i -th level structure³⁷⁻⁴⁰. If the interface has finite interfacial thickness, q^{-4} is modified to be $q^{-4} \exp(-t_1^2 q^2 / 2)$, where t_1 is the interfacial thickness. For a surface fractal,

$$B_i = 4\rho^2 \Delta a^2 R_{g,i}^{(6-P_i)} G \left((P_i - 1) \sin\left(\rho(P_i - 3)/2\right) \right) (P_i - 3) \quad (4)$$

and $P_i = 6 - d_s$, where d_s is the surface fractal dimension⁴¹. For a mass fractal structure, $P_i = d_f$, where d_f is the mass fractal dimension and $1 < d_f < 3$. B_i is expressed by

$$B_i = \frac{G_i d_{\min}}{R_{g,i}^{d_f}} G\left(\frac{d_f}{2}\right) \quad (5)$$

if the i -th level structure or aggregation is monodisperse^{42,43}. In eq. (5), d_{\min} is called the minimum dimension and $d_{\min} = d_f$ if the aggregation is linear. For a Gaussian chain, B_i is given by

$$B_i = \frac{2G_i}{R_{g,i}^2} \quad (6)$$

while

$$B_i = \frac{G_i}{R_{g,i}^2} \quad (7)$$

for a disk. The parameter c is defined by

$$c = \frac{d_{\min}}{d_f} \quad (8)$$

which characterizes the degree of branching and is estimated from B_i , d_f , and $R_{g,i}$, which are determined by fitting the experimental scattering profiles⁴³.

When the aggregation is polydisperse, B_i is given by

$$B_i = \frac{G_i A}{R_{g,i}^{d_f}} G\left(\frac{d_f}{2}\right)$$

(9)

and A characterizes the polydispersity of the aggregation. For the branched polydisperse aggregates, it is not possible to isolate the effects of dispersion from branching⁴³.

Percus-Yevick approximation with an upper limit

In some rubber-filler systems, such as aggregates of silica particles, the primary particles interact with each other, and a liquid-like correlation is formed in the aggregations. In such cases, we can employ the Percus-Yevick approximation to calculate the correlations and the scattering functions of the primary particles. Moreover, we must impose the upper limit, which is characterized by the aggregate size, on the scattering function.

For monodisperse systems with spherically symmetric particle shapes and interactions, the scattered intensity can be written as^{7,37}

$$I(q) = n_p D a^2 V_p^2 P(q) S(q), \quad (10)$$

where n_p is the number density of particles, V_p is the volume of the primary particle, $P(q)$ is the form factor of the primary particle with radius R , and $S(q)$ is the structure

factor. For dilute systems, $S(q) = 1$. The form factors for typical structures have been calculated and are listed in the review written by Pedersen⁴⁴. For example, the form factor $P(q, R)$ for a sphere with radius R is given by

$$P(q) = \frac{9[\sin(qR) - qR\cos(qR)]^2}{(qR)^6}. \quad (11)$$

We can obtain the analytical form of $S(q, R_{HS})$ using the Percus-Yevick approximation for the hard-sphere model with an interaction radius R_{HS} .^{45,46}

$$S(q, R_{HS}) = \frac{1}{1 + 24fG(R_{HS}q)/(R_{HS}q)} \quad (12)$$

Here,

$$G(A) = a(\sin A - A \cos A)/A^2 + b(2A \sin A + (2 - A^2)\cos A - 2)/A^3 \\ + g[-A^4 \cos A + 4\{(3A^2 - 6)\cos A + (A^3 - 6A)\sin A + 6\}]/A^5 \quad (13)$$

and

$$a = (1 - 2f)^2/(1 - f)^4 \quad (14)$$

$$b = -6f(1 + f/2)^2/(1 - f)^2 \quad (15)$$

$$g = af/2. \quad (16)$$

For the polydisperse case, we cannot write the scattered intensity as a product of the form factor and the structure factor; hence, it is necessary to calculate the following equation:

$$I(q) = Da^2 \left[\int_0^\infty N(r) V(r)^2 F(q, r)^2 dr + \int_0^\infty \int_0^\infty N(r) V(r) N(r') V(r') F(q, r) F(q, r') S(q, r, r') dr dr' \right]. \quad (17)$$

In eq. (17), $N(r)$ is the number density of a particle with radius r , $V(r)$ is the volume of a particle with radius r , $F(q, r)$ is the amplitude of the form factor with r , and $S(q, r, r')$ is the partial structure factor. Vrij⁴⁷, Blum and Stell⁴⁸, Salacuse and Stell⁴⁹, and Griffith et al.⁵⁰ presented the analytical scattering functions for polydisperse systems. However, this scattering function is not suitable for analyzing the experimental data. Thus, the approximated equations are usually used to analyze the experimental data. For low-volume fractions, the decoupling approximation⁵¹ given by Chen et al. is applicable:

$$I(q) = n_p Da^2 \left[\langle V(r)^2 F(q, r)^2 \rangle + \langle V(r) F(q, r) \rangle^2 S(q, \langle r^3 \rangle^{1/3}) \right] \quad (18)$$

where $\langle \rangle$ denotes the first moment with respect to the size distribution and $S(q, r)$ is given by eqs. (12) to (16). For dense systems, the local monodisperse approximation

proposed by Pedersen⁵² is effective:

$$I(q) = n_p D a^2 \int_0^\infty N(r) V(r)^2 F(q, r)^2 S(q, R_{HS}(r)) dr \quad (19)$$

where $R_{HS}(r) = r$ for particles interacting with their actual radius.

The scattering functions described above do not include the upper limit of the aggregation. Here, we shall introduce the upper limit using paracrystal theory⁵³. For simplicity, we consider the monodisperse systems with spherical symmetry of the particle shapes and the interactions. The structure factor $S(q)$ is expressed with the radial distribution function $g(r)$ by

$$S(q) = 1 + n_p \int_0^\infty g(r) \frac{\sin qR}{qr} 4\pi r^2 dr, \quad (20)$$

Substituting

$$g(r) = 1 + [g(r) - 1] \quad (21)$$

into eq. (20) to separate the scattering of the homogeneous portion, we can then obtain^{37,54,55}

$$\begin{aligned} S(q) &= 1 + n_p \int_0^\infty \frac{\sin qR}{qr} 4\rho r^2 dr + n_p \int_0^\infty [g(r) - 1] \frac{\sin qR}{qr} 4\rho r^2 dr \\ &= 1 + n_p \mathcal{D}(q) + n_p \int_0^\infty [g(r) - 1] \frac{\sin qR}{qr} 4\rho r^2 dr, \end{aligned} \quad (22)$$

where $\delta(q)$ is the delta function. We usually omit either the homogeneous part or $\delta(q)$ and define $S(q)$ as

$$S(q) = 1 + n_p \int_0^\infty [g(r) - 1] \frac{\sin qR}{qr} 4\rho r^2 dr, \quad (23)$$

because $\delta(q)=0$ at $q \neq 0$. However, we must leave the term so that we can include the upper limit. Thus, we define $S(q)$ including $\delta(q)$ as $S_T(q)$:

$$S_T(q) = 1 + n_p \mathcal{D}(q) + n_p \int_0^\infty [g(r) - 1] \frac{\sin qR}{qr} 4\rho r^2 dr = n_p \mathcal{D}(q) + S(q). \quad (24)$$

According to paracrystal theory⁵³, the scattering function affected by the shape of the aggregation is given by

$$I(q) = n_p D a^2 V_p^2 P(q) S_T(q) * G(q) \quad (25)$$

where $G(q)$ is the structure factor of the aggregation and $*$ denotes the convolution product. Substituting eq. (24) into eq. (25), we obtain

$$\begin{aligned}
 I(q) &= n_p D a^2 V_p^2 P(q) \left[n_p d(q) + 1 + n_p \int_0^\infty [g(r) - 1] \frac{\sin qR}{qr} 4\pi r^2 dr \right] * G(q) \\
 &= n_p D a^2 V_p^2 P(q) [n_p d(q) + S(q)] * G(q) \\
 &= n_p D a^2 V_p^2 P(q) [n_p G(q) + S(q) * G(q)].
 \end{aligned} \tag{26}$$

In this equation, $G(q)$ is dominant at smaller q -regions, while

$$I(q) \approx n_p D a^2 V_p^2 P(q) S(q) \tag{27}$$

at higher q regions because $G(q)$ is approximated by $\delta(q)$ at higher q regions. With $G(q)$, we can use the Debye-Bueche equation⁵⁶. If the correlation function of $G(q)$ and $S(q)$ are known, $S(q) * G(q)$ is obtained by taking the Fourier transform of the products of the correlation functions.

By using the Percus-Yevick approximation with the upper limit, we can calculate the scattering function of the aggregations. We can incorporate the scattering function into the unified Guinier/power-law as a scattering function for one level of the hierarchical structure.

The reverse Monte Carlo method

The reverse Monte Carlo method has been effectively used to construct a possible structure in real space from its corresponding scattering function. For rubber-filler

systems, the aggregation of primary silica particles has been investigated with the reverse Monte Carlo method, and real space images were obtained for the aggregations of silica particles⁵⁷⁻⁶¹.

Hagita et al. developed a two-dimensional pattern reverse Monte Carlo method for the analysis of two-dimensional scattering patterns^{62,63}. They applied the method to the investigation of structural changes in silica particle filler under uniaxial elongation. From this, they calculated three-dimensional conformations of the spherical silica particles using a series of two-dimensional patterns of structure factors obtained by Shinohara et al. during elongation. They successfully obtained the deformation of the network structure formed by the silica fillers^{21,64}.

However, all procedures do not consider all levels of the hierarchical structure. Thus, we must eliminate the effects of the higher or lower level structures from the scattering function to quantitatively analyze the experimental data with reverse Monte Carlo methods.

Contrast variation SANS for the analysis of adsorption layers around fillers

The contrast variation SANS method has been developed by Endo⁶⁵⁻⁶⁸. We applied contrast variation SANS to the investigation of the adsorbed rubber layer around the silica particles and the carbon black^{69,70}. To enhance the adsorption layer, we swell the rubber-filler systems with solvent. The swollen ratio of the adsorbed layers is smaller than that of the matrix phase, and the scattering contrast between the adsorption layers

and the matrix phase is caused by the difference in the swollen ratio. The swollen rubber-filler system can be treated as a three-component system, and their scattering profiles can be described as follows under an incompressible condition:

$$I(q) = (a_R - a_S)^2 S_{RR}(q) + (a_R - a_S)(a_F - a_S) S_{RF}(q) + (a_F - a_S)^2 S_{FF}(q). \quad (28)$$

Here, a_i is the scattering length density of the i -th component ($i = R$: rubber, F : filler, and S : solvent). $S_{ij}(q)$ is the partial scattering function defined by

$$S_{ij}(q) = \frac{1}{V} \iint_V (df_i(\vec{r}) df_j(\vec{r}')) \exp[i\vec{q}(\vec{r} - \vec{r}')] d\vec{r} d\vec{r}', \quad (29)$$

where V is the scattering volume irradiated by the incident beam and $df_i(\vec{r})$ is the fluctuation of the volume fraction of i at position \vec{r} . We can obtain the vector of the scattering intensities $\vec{I} = [I_1(q), I_2(q), \dots, I_n(q)]$ from the same samples with n different scattering length densities of S . The partial structure factors can be obtained by

$$\vec{S} = \mathbf{M}^T \times \vec{I}, \quad (30)$$

where the transposed matrix \mathbf{M}^T satisfies $\mathbf{M}^T \times \mathbf{M} = \mathbf{E}$ by singular value decomposition, \mathbf{M} is the matrix of the difference in the scattering length density, and

\vec{S} is the vector of the partial scattering functions. For three-component systems, \mathbf{M} is expressed by

$$\mathbf{M} = \begin{pmatrix} {}^1\mathbb{D}a_R^2 & {}^1\mathbb{D}a_R \cdot {}^1\mathbb{D}a_F & {}^1\mathbb{D}a_F^2 \\ {}^2\mathbb{D}a_R^2 & {}^2\mathbb{D}a_R \cdot {}^2\mathbb{D}a_F & {}^2\mathbb{D}a_F^2 \\ \vdots & \vdots & \vdots \\ {}^n\mathbb{D}a_R^2 & {}^n\mathbb{D}a_R \cdot {}^n\mathbb{D}a_F & {}^n\mathbb{D}a_F^2 \end{pmatrix}, \quad (31)$$

where

$${}^n\mathbb{D}a_R = a_R - {}^na_S \quad (32)$$

and

$${}^n\mathbb{D}a_F = a_F - {}^na_S. \quad (33)$$

\vec{S} is given by

$$\vec{S} = \begin{pmatrix} S_{RR}(q) \\ S_{RF}(q) \\ S_{FF}(q) \end{pmatrix}. \quad (34)$$

$S_{FF}(q)$ is the scattered intensity of the aggregate filler structure, while $S_{RR}(q)$ and $S_{RF}(q)$ are affected by the adsorption layer. To analyze the adsorption layer, a three-phase model consisting of the filler aggregation, the adsorption layer and the matrix phase is proposed. The application of this method is shown later.

APPLICATIONS

Analysis of the hierarchical structures of fillers

Koga et al. measured the scattering function of carbon black (CB, SHOBLOCK N339, Showa Cabot, Chiba, Japan) / poly(styrene-random-butadiene) copolymer (SBR, weight-averaged molecular weight $M_w=5.0 \times 10^5$, weight fraction of styrene content $w_{PS}=0.235$) systems using the combined scattering method, including USANS, USAXS and SAXS, as shown in Figure 5, in which the volume fraction of CB is $0.20^{71,72}$. They found that the scattering function of CB/SBR can be well-described by the following the unified Guinier/power-law equation:

$$\begin{aligned}
 I(q) = & A \exp\left(-q^2 R_{gg}^2/3\right) q^{-4} \\
 & + B \exp\left(-q^2 R_{gg}^2/3\right) + C \exp\left(-q^2 R_{SS}^2/3\right) \times \left[\operatorname{erf}\left(q R_{gg}/\sqrt{6}\right)^3 / q \right]^{2.3} \\
 & + D \exp\left(-q^2 R_{SS}^2/3\right) + E \left[\operatorname{erf}\left(q R_{SS}/\sqrt{6}\right)^3 / q \right]^{6-D_S}.
 \end{aligned} \tag{35}$$

The fitting results and transmission electron microscope observations of the primary particles indicate that the hierarchical structure consists of the following structural levels, in increasing order of the length scale: the primary CB particles where the radius of the primary particles is 13 nm and the surface fractal structure is $D_S=2.6$; the aggregates comprising approximately 9 fused primary CB particles and $R_{SS} = 27$ nm;

the agglomerate or the mass-fractal objects formed by the aggregates with $D_m = 2.3$ and $R_{gg} = 2.0 \mu\text{m}$; and the bulk rubber composed of a dispersion of the mass-fractal objects in the cross-linked bulk rubbers. Moreover, they found either another hierarchical structure or dispersible units between the aggregates and the agglomerates and that the morphologies of the dispersible units are an ellipsoid of revolution by investigating the detail of the scattering profiles around the Guinier region. The hierarchical structure of the SBR/CB system is summarized in Figure 6.

There are reports on applications of the unified Guinier/power-law method to silica rubber systems, precipitated silica powders, and nano-composites⁷³⁻⁷⁸. Silica-rubber systems also form hierarchical structures consisting of agglomerates, aggregates and particles, and the size of each structure can be estimated from the scattering function. Moreover, we can estimate the size distribution of silica particles⁷⁵. Schaefer et al. investigated the hierarchical structures of the precipitated silica prepared by the acidification of water glass using light scattering, USAXS, SAXS, and WAXS, which cover the range from 3×10^{-6} to 50 nm^{-1} , as shown in Figure 7⁷⁷. By fitting four levels of the unified Guinier/power-law equation to the scattering function at $3 \times 10^{-6} < q < 4 \text{ nm}^{-1}$, they found that the hierarchical structure consists of agglomerate level 2 ($R_g = 115 \mu\text{m}$, $D_m=1.9$, mass fractal), agglomerate level 1 ($R_g = 0.9 \mu\text{m}$, $D_s=2.8$, rough surface), aggregates ($R_g = 66 \text{ nm}$, $D_m=1.8$, mass fractal), and particles ($R_g = 4.7 \text{ nm}$, $D_s=2$ or Porod law, smooth surface)⁷⁵.

In situ measurement of the time-resolved 2D-USAXS of the rubber-filler systems

under deformation

Shinohara et al. investigated the change in the structures of SBR/silica systems with elongation using time-resolved 2D-USAXS²¹. As shown in Figure 8, they successfully measured 2D-USAXS patterns and stress-strain curves simultaneously. They found that the distance between the silica particles increases with strain but that the distance between the silica particles connected with polymer chains remained constant. As mentioned above, Hagita et al. reconstructed the three-dimensional conformations of spherical silica particles from 2D-USAXS patterns during elongation using the reverse Monte Carlo method^{62,63}.

Analyses of the adsorption layers around fillers with contrast variation SANS

We measured the scattering intensities of silica/SBR (systems swollen by mixtures of deuterated hexane (d-hex) and hexane (h-hex)) with various scattering length densities, as shown in Figure 9⁶⁹. By using eqs. (30) to (33), we obtained partial scattering functions, as shown in Figure 10: the scattering function for the polymer-polymer correlation $S_{PP}(q)$, the scattering function for the silica-silica correlation $S_{SS}(q)$, and the scattering function for the polymer-silica correlation $S_{PS}(q)$. The analyses of $S_{SS}(q)$ explored the hierarchical structures formed by silica particles. The analyses of $S_{PS}(q)$ and $S_{SS}(q)$ clarified the existence of dense polymer layers around the silica aggregates. Several characteristic parameters are estimated from the analysis, such as the size of the aggregates, the thickness of the layers, the volume fractions of the polymer layers and the matrix, and the correlation length of the matrix network. We compared the volume fraction f_m of polymer in the matrix estimated from the SANS experiment with that

from the degree of swelling and explored the agreement between them. We also estimated that the aggregation consists of 91 silica particles. Additionally, we applied this method to the SBR/CB systems⁷⁰ and found that the thickness of the dense polymer layers in the SBR/CB system is larger than that of the SBR/silica system.

CONCLUSION

I have described recent progress in the analysis of the hierarchical structures formed in rubber-filler systems using combined scattering methods. Because the development of ultra-small-angle scattering has covered $10^{-4} < q < 10^{-2} \text{ nm}^{-1}$, we can quantitatively characterize hierarchical structures over a wide range of length scales, ranging from nanometers to micrometers, by combining SAXS, SANS, and WAXS. It should be noted that both USAXS with a long camera path and focusing SANS are powerful tools for the analysis of change in the structures under deformation. The scattering theories for the analysis of the experimental scattering functions are summarized. The unified Guinier/power-law method can describe the scattering profiles of the rubber-filler systems with hierarchical structures. In situ 2D-USAXS measurements of the rubber-filler system under elongation can explore the deformation in the hierarchical structures. Contrast variation SANS can evaluate the interfacial properties in the rubber-filler systems.

I have not mentioned the analysis of the network structure of rubber by scattering methods, but this is an important subject in rubber-filler systems⁷⁹⁻⁸¹. In particular, the inhomogeneity of the network at the micron scale should be clarified.

We should explore the relationships among the mechanical properties, the structures and the compounding conditions in rubber-filler systems, which are not yet fully understood.

ACKNOWLEDGMENTS

I would like to thank Dr. Amino Naoya, Dr. Yasuhiro Ishikawa, Professor Tadanori Koga, Dr. Daisuke Yamaguchi, Professor Satoshi Koizumi, Professor Shotaro Nishitsuji, Mr. Toyohisa Tohyama, and Mr. Kiyotaka Kadomachi for their collaboration. I would like to express my gratitude to Dr. Hitoshi Endo, Dr. Masugu Sato, Dr. Naoto Yagi, Dr. Yoshio Suzuki, Dr. Akihisa Takeuchi, Professor Takeji Hashimoto, Dr. Hiroki Murase, and Professor Masaki Takata for providing invaluable discussion and comments.

REFERENCES

- 1 Boonstra, B. B. Role of Particulate Fillers in Elastomer Reinforcement - Review. *Polymer* **20**, 691-704, (1979).
- 2 Eggers, H. & Schummer, P. Reinforcement mechanisms in carbon black and silica loaded rubber melts at low stresses. *Rubber Chem Technol* **69**, 253-265, (1996).
- 3 Eirich, F. R. & American Chemical Society, R. D. *Science and technology of rubber*. (Academic Press, 1978).
- 4 Heinrich, G. *Advanced Rubber Composites*. Vol. 238 (Springer-Verlag, 2011).
- 5 Kraus, G. *Reinforcement of Elastomers*. (Interscience Publishers, 1965).
- 6 Nielsen, L. E. *Mechanical properties of polymers and composites*. Vol. . 1 (M. Dekker, 1974).
- 7 Roe, R. J. *Methods of X-ray and neutron scattering in polymer science*. (Oxford University Press, 2000).
- 8 Ikeda, Y., Yasuda, Y., Hijikata, K., Tosaka, M. & Kohjiya, S. Comparative study on strain-induced crystallization behavior of peroxide cross-linked and sulfur cross-linked natural rubber. *Macromolecules* **41**, 5876-5884, (2008).
- 9 Saijo, K., Zhu, Y.-P., Hashimoto, T., Wasiak, A. & Brzostowski, N. Oriented crystallization of crosslinkedcis-1,4-polybutadiene rubber. *Journal of Applied Polymer Science* **105**, 137-157, (2007).
- 10 Toki, S., Sics, I., Hsiao, B. S., Tosaka, M., Poompradub, S., Ikeda, Y. & Kohjiya, S. Probing the nature of strain-induced crystallization in polyisoprene rubber by

- combined thermomechanical and in situ X-ray diffraction techniques. *Macromolecules* **38**, 7064-7073, (2005).
- 11 Rathje, J. & Ruland, W. Density Fluctuations in Amorphous and Semicrystalline Polymers. *Colloid Polym Sci* **254**, 358-370, (1976).
 - 12 Vonk, C. G. Investigation of Non-Ideal 2-Phase Polymer Structures by Small-Angle X-Ray-Scattering. *J Appl Crystallogr* **6**, 81-86, (1973).
 - 13 Hashimoto, T., Fujimura, M. & Kawai, H. Domain-Boundary Structure of Styrene-Isoprene Block Co-Polymer Films Cast from Solutions .5. Molecular-Weight Dependence of Spherical Microdomains. *Macromolecules* **13**, 1660-1669, (1980).
 - 14 Hashimoto, T., Shibayama, M. & Kawai, H. Domain-Boundary Structure of Styrene-Isoprene Block Co-Polymer Films Cast from Solution .4. Molecular-Weight Dependence of Lamellar Microdomains. *Macromolecules* **13**, 1237-1247, (1980).
 - 15 Higgins, J. S. & Benoît, H. *Polymers and neutron scattering*. (Clarendon Press; Oxford University Press, 1994).
 - 16 Bonse, U. & Hart, M. Tailless X-Ray Single-Crystal Reflection Curves Obtained by Multiple Reflection - (Si Ge Crystals - E/T). *Appl Phys Lett* **7**, 238-&, (1965).
 - 17 Koga, T., Hart, M. & Hashimoto, T. Development of a high-flux- and high-temperature-set-up Bonse-Hart ultra-small-angle X-ray scattering (USAXS) diffractometer. *J Appl Crystallogr* **29**, 318-324, (1996).
 - 18 Narayanan, T., Diat, O. & Bosecke, P. SAXS and USAXS on the high brilliance

- beamline at the ESRF. *Nucl Instrum Meth A* **467**, 1005-1009, (2001).
- 19 Sztucki, M. & Narayanan, T. Development of an ultra-small-angle X-ray scattering instrument for probing the microstructure and the dynamics of soft matter. *J Appl Crystallogr* **40**, S459-S462, (2007).
- 20 Ilavsky, J., Jemian, P. R., Allen, A. J., Zhang, F., Levine, L. E. & Long, G. G. Ultra-small-angle X-ray scattering at the Advanced Photon Source. *J Appl Crystallogr* **42**, 469-479, (2009).
- 21 Shinohara, Y., Kishimoto, H., Inoue, K., Suzuki, Y., Takeuchi, A., Uesugi, K., Yagi, N., Muraoka, K., Mizoguchi, T. & Amemiya, Y. Characterization of two-dimensional ultra-small-angle X-ray scattering apparatus for application to rubber filled with spherical silica under elongation. *J Appl Crystallogr* **40**, S397-S401, (2007).
- 22 Yagi, N. & Inoue, K. Ultra-small-angle X-ray diffraction and scattering experiments using medium-length beamlines at SPring-8. *J Appl Crystallogr* **36**, 783-786, (2003).
- 23 BL19B2. <http://support.spring8.or.jp/en/usax-e.html>.
- 24 Agamalian, M., Wignall, G. D. & Triolo, R. Optimization of a Bonse-Hart Ultra-Small-Angle Neutron Scattering facility by elimination of the rocking-curve wings. *J Appl Crystallogr* **30**, 345-352, (1997).
- 25 Aizawa, K. & Tomimitsu, H. Design and Use of a Double-Crystal Diffractometer for Very Small-Angle Neutron-Scattering at Jrr-3m. *Physica B* **213**, 884-886, (1995).

- 26 Schwahn, D., Miksovsky, A., Rauch, H., Seidl, E. & Zugarek, G. Test of Channel-Cut Perfect Crystals for Neutron Small-Angle Scattering Experiments. *Nucl Instrum Meth A* **239**, 229-234, (1985).
- 27 Yamaguchi, D., Koizumi, S., Motokawa, R., Kumada, T., Aizawa, K. & Hashimoto, T. Tandem analyzer crystals system doubles counting rate for Bonse-Hart ultra-small-angle neutron-scattering spectrometer. *Physica B* **385-86**, 1190-1193, (2006).
- 28 Choi, S. M., Barker, J. G., Glinka, C. J., Cheng, Y. T. & Gammel, P. L. Focusing cold neutrons with multiple biconcave lenses for small-angle neutron scattering. *J Appl Crystallogr* **33**, 793-796, (2000).
- 29 Koizumi, S., Iwase, H., Suzuki, J., Oku, T., Motokawa, R., Sasao, H., Tanaka, H., Yamaguchi, D., Shimizu, H. M. & Hashimoto, T. Focusing and polarized neutron ultra-small-angle scattering spectrometer (SANS-J-II) at Research Reactor JRR3, Japan. *Physica B* **385-86**, 1000-1006, (2006).
- 30 Koizumi, S., Iwase, H., Suzuki, J. I., Oku, T., Motokawa, R., Sasao, H., Tanaka, H., Yamaguchi, D., Shimizu, H. M. & Hashimoto, T. Focusing and polarized neutron small-angle scattering spectrometer (SANS-J-II). The challenge of observation over length scales from an angstrom to a micrometre. *J Appl Crystallogr* **40**, S474-S479, (2007).
- 31 Iwase, H., Endo, H., Katagiri, M. & Shibayama, M. Modernization of the small-angle neutron scattering spectrometer SANS-U by upgrade to a focusing SANS spectrometer. *J Appl Crystallogr* **44**, 558-568, (2011).

- 32 Alefeld, B., Hayes, C., Mezei, F., Richter, D. & Springer, T. High-resolution focusing SANS with a toroidal neutron mirror. *Physica B* **234**, 1052-1054, (1997).
- 33 Brulet, A., Thevenot, V., Lairez, D., Lecommandoux, S., Agut, W., Armes, S. P., Du, J. Z. & Desert, S. Toward a new lower limit for the minimum scattering vector on the very small angle neutron scattering spectrometer at Laboratoire Leon Brillouin. *J Appl Crystallogr* **41**, 161-166, (2008).
- 34 Grunzweig, C., Hils, T., Muhlbauer, S., Ay, M., Lorenz, K., Georgii, R., Gahler, R. & Boni, P. Multiple small angle neutron scattering: A new two-dimensional ultrasmall angle neutron scattering technique. *Appl Phys Lett* **91**, (2007).
- 35 Beaucage, G. Approximations leading to a unified exponential power-law approach to small-angle scattering. *J Appl Crystallogr* **28**, 717-728, (1995).
- 36 Beaucage, G. & Schaefer, D. W. Structural Studies of Complex-Systems Using Small-Angle Scattering - a Unified Guinier Power-Law Approach. *J Non-Cryst Solids* **172**, 797-805, (1994).
- 37 Guinier, A., Fournet, G., Walker, C. B. F. & Yudowitch, K. L. *Small-angle scattering of X-rays*. (In-house reproduction, 1955).
- 38 Porod, G. Die Röntgenkleinwinkelstreuung Von Dichtgepackten Kolloiden Systemen .1. *Kolloid Z Z Polym* **124**, 83-114, (1951).
- 39 Porod, G. Die Röntgenkleinwinkelstreuung Von Dichtgepackten Kolloiden Systemen .2. *Kolloid Z Z Polym* **125**, 51-57, (1952).
- 40 Porod, G. Die Röntgenkleinwinkelstreuung Von Dichtgepackten Kolloiden

- Systemen .2. *Kolloid Z Z Polym* **125**, 108-122, (1952).
- 41 Bale, H. D. & Schmidt, P. W. Small-Angle X-Ray-Scattering Investigation of Submicroscopic Porosity with Fractal Properties. *Phys Rev Lett* **53**, 596-599, (1984).
 - 42 Beaucage, G. Small-angle scattering from polymeric mass fractals of arbitrary mass-fractal dimension. *J Appl Crystallogr* **29**, 134-146, (1996).
 - 43 Beaucage, G. Determination of branch fraction and minimum dimension of mass-fractal aggregates. *Phys Rev E* **70**, (2004).
 - 44 Pedersen, J. S. Analysis of small-angle scattering data from colloids and polymer solutions: modeling and least-squares fitting. *Adv Colloid Interfac* **70**, 171-210, (1997).
 - 45 Kinning, D. J. & Thomas, E. L. Hard-Sphere Interactions between Spherical Domains in Diblock Copolymers. *Macromolecules* **17**, 1712-1718, (1984).
 - 46 Wertheim, M. S. Exact Solution of Percus-Yevick Integral Equation for Hard Spheres. *Phys Rev Lett* **10**, 321-&, (1963).
 - 47 Vrij, A. Mixtures of Hard-Spheres in the Percus-Yevick Approximation - Light-Scattering at Finite Angles. *J Chem Phys* **71**, 3267-3270, (1979).
 - 48 Blum, L. & Stell, G. Polydisperse Systems .1. Scattering Function for Polydisperse Fluids of Hard or Permeable Spheres. *J Chem Phys* **71**, 42-46, (1979).
 - 49 Salacuse, J. J. & Stell, G. Polydisperse Systems - Statistical Thermodynamics, with Applications to Several Models Including Hard and Permeable Spheres. *J*

- Chem Phys* **77**, 3714-3725, (1982).
- 50 Griffith, W. L., Triolo, R. & Compere, A. L. Analytical Scattering Function of a Polydisperse Percus-Yevick Fluid with Schulz-(Gamma-) Distributed Diameters. *Phys Rev A* **35**, 2200-2206, (1987).
- 51 Kotlarchyk, M. & Chen, S. H. Analysis of Small-Angle Neutron-Scattering Spectra from Polydisperse Interacting Colloids. *J Chem Phys* **79**, 2461-2469, (1983).
- 52 Pedersen, J. S. Determination of Size Distributions from Small-Angle Scattering Data for Systems with Effective Hard-Sphere Interactions. *J Appl Crystallogr* **27**, 595-608, (1994).
- 53 Hosemann, R. & Bagchi, S. N. *Direct analysis of diffraction by matter*. (North-Holland Pub. Co, 1962).
- 54 Debye, P. & Menke, H. Bestimmung der inneren Struktur von Flüssigkeiten mit Röntgenstrahlen. *Physik. Zeitschr.* **31**, 797-798, (1930).
- 55 Zernike, F. & Prins, J. A. Die Beugung von Röntgenstrahlen an Flüssigkeiten als Effekt der Molekülanordnung. *Z. Physik* **41**, 184-194, (1927).
- 56 Debye, P. & Bueche, A. M. Scattering by an Inhomogeneous Solid. *J Appl Phys* **20**, 518-525, (1949).
- 57 Gereben, O., Pusztai, L. & McGreevy, R. L. RMCSANS-modelling the inter-particle term of small angle scattering data via the reverse Monte Carlo method. *J Phys-Condens Mat* **22**, (2010).
- 58 Oberdisse, J. Aggregation of colloidal nanoparticles in polymer matrices. *Soft*

- Matter* **2**, 29-36, (2006).
- 59 Oberdisse, J., Hine, P. & Pyckhout-Hintzen, W. Structure of interacting aggregates of silica nanoparticles in a polymer matrix: small-angle scattering and reverse Monte Carlo simulations. *Soft Matter* **3**, 476-485, (2007).
 - 60 Pusztai, L., Dominguez, H. & Pizio, O. A. Reverse Monte Carlo modeling of the structure of colloidal aggregates. *J Colloid Interf Sci* **277**, 327-334, (2004).
 - 61 Toth, G. Monte Carlo determination of the radii and the pair-correlation function of spherical colloids. *Physica B* **276**, 404-405, (2000).
 - 62 Hagita, K., Arai, T., Kishimoto, H., Umesaki, N., Shinohara, Y. & Amemiya, Y. Two-dimensional pattern reverse Monte Carlo method for modelling the structures of nano-particles in uniaxial elongated rubbers. *J Phys-Condens Mat* **19**, (2007).
 - 63 Hagita, K., Arai, T., Kishimoto, H., Umesaki, N., Suno, H., Shinohara, Y. & Amemiya, Y. Structural changes of silica particles in elongated rubber by two-dimensional small-angle X-ray scattering and extended reverse Monte Carlo analysis. *Rheol Acta* **47**, 537-541, (2008).
 - 64 Kishimoto, H., Shinohara, Y., Amenya, Y., Inoue, K., Suzuki, Y., Takeuchi, A., Uesugi, K. & Yagi, N. Structural Analysis of Filler in Rubber Composite under Stretch with Time-Resolved Two-Dimensional Ultra-Small-Angle X-Ray Scattering. *Rubber Chem Technol* **81**, 541-551, (2008).
 - 65 Endo, H., Allgaier, J., Gompper, G., Jakobs, B., Monkenbusch, M., Richter, D., Sottmann, T. & Strey, R. Membrane decoration by amphiphilic block

- copolymers in bicontinuous microemulsions. *Phys Rev Lett* **85**, 102-105, (2000).
- 66 Endo, H., Schwahn, D. & Colfen, H. On the role of block copolymer additives for calcium carbonate crystallization: Small angle neutron scattering investigation by applying contrast variation. *J Chem Phys* **120**, 9410-9423, (2004).
- 67 Miyazaki, S., Endo, H., Karino, T., Haraguchi, K. & Shibayama, M. Gelation mechanism of poly(N-isopropylacrylamide)-clay nanocomposite gels. *Macromolecules* **40**, 4287-4295, (2007).
- 68 Suzuki, T., Endo, H. & Shibayama, M. Analysis of surface structure and hydrogen/deuterium exchange of colloidal silica suspension by contrast-variation small-angle neutron scattering. *Langmuir* **24**, 4537-4543, (2008).
- 69 Takenaka, M., Nishitsuji, S., Amino, N., Ishikawa, Y., Yamaguchi, D. & Koizumi, S. Structure Analyses of Swollen Rubber-Filler Systems by Using Contrast Variation SANS. *Macromolecules* **42**, 308-311, (2009).
- 70 Takenaka, M., Nishitsuji, S., Amino, N., Ishikawa, Y., Yamaguchi, D. & Koizumi, S. Structure Analyses of Swollen Rubber-Carbon Black Systems by Using Contrast Variation Small-Angle Neutron Scattering. *Rubber Chem Technol* **85**, 157-164, (2012).
- 71 Koga, T., Hashimoto, T., Takenaka, M., Aizawa, K., Amino, N., Nakamura, M., Yamaguchi, D. & Koizumi, S. New insight into hierarchical structures of carbon black dispersed in polymer matrices: A combined small-angle scattering study.

- Macromolecules* **41**, 453-464, (2008).
- 72 Koga, T., Takenaka, M., Aizawa, K., Nakamura, M. & Hashimoto, T. Structure factors of dispersible units of carbon black filler in rubbers. *Langmuir* **21**, 11409-11413, (2005).
- 73 Fresnais, J., Berret, J. F., Qi, L., Chapel, J. P., Castaing, J. C., Sandre, O., Frka-Petesic, B., Perzynski, R., Oberdisse, J. & Cousin, F. Universal scattering behavior of coassembled nanoparticle-polymer clusters. *Phys Rev E* **78**, (2008).
- 74 Schaefer, D. W. & Agamalian, M. M. Ultra-small-angle neutron scattering: a new tool for materials research. *Curr Opin Solid St M* **8**, 39-47, (2004).
- 75 Schaefer, D. W. & Chen, C. Y. Structure optimization in colloidal reinforcing fillers: Precipitated silica. *Rubber Chem Technol* **75**, 773-793, (2002).
- 76 Schaefer, D. W. & Justice, R. S. How nano are nanocomposites? *Macromolecules* **40**, 8501-8517, (2007).
- 77 Schaefer, D. W., Rieker, T., Agamalian, M., Lin, J. S., Fischer, D., Sukumaran, S., Chen, C. Y., Beaucage, G., Herd, C. & Ivie, J. Multilevel structure of reinforcing silica and carbon. *J Appl Crystallogr* **33**, 587-591, (2000).
- 78 Schaefer, D. W., Suryawanshi, C., Pakdel, P., Ilavsky, J. & Jemian, P. R. Challenges and opportunities in complex materials: silica-reinforced elastomers. *Physica a-Statistical Mechanics and Its Applications* **314**, 686-695, (2002).
- 79 Ikeda, Y., Higashitani, N., Hijikata, K., Kokubo, Y., Morita, Y., Shibayama, M., Osaka, N., Suzuki, T., Endo, H. & Kohjiya, S. Vulcanization: New Focus on a Traditional Technology by Small-Angle Neutron Scattering. *Macromolecules* **42**,

2741-2748, (2009).

- 80 Karino, T., Ikeda, Y., Yasuda, Y., Kohjiya, S. & Shibayama, M. Nonuniformity in natural rubber as revealed by small-angle neutron scattering, small-angle X-ray scattering, and atomic force microscopy. *Biomacromolecules* **8**, 693-699, (2007).
- 81 Suzuki, T., Osaka, N., Endo, H., Shibayama, M., Ikeda, Y., Asai, H., Higashitani, N., Kokubo, Y. & Kohjiya, S. Nonuniformity in Cross-Linked Natural Rubber as Revealed by Contrast-Variation Small-Angle Neutron Scattering. *Macromolecules* **43**, 1556-1563, (2010).

FIGURE CAPTIONS

- Figure 1 q - and length-scales covered by various scattering methods, and the hierarchical structure of rubber-filler systems.
- Figure 2 Side view of the optical set-up of the Bonse-Hart USAXS¹⁷.
- Figure 3 Schematic view of the experimental set-up of USAXS at BL20XU²¹.
- Figure 4 Schematic diagram for focusing collimation with compound lenses in which L_s 1/4 9.6 m, L_1 1/4 8.1–8.7 and L_2 1/4 11–11.6 m³⁰.
- Figure 5 A combination of the USANS, USAXS, and SAXS profiles for CB/ SBR (open circles). R_{SS} and R_{gg} correspond to the sizes of the aggregates and the agglomerates, respectively. The solid line is the best-fitted theoretical scattering profile expressed by eq. (35)⁷¹.
- Figure 6 Schematic model of the hierarchical structure of CB/ SBR⁷¹.
- Figure 7 Scattering profile of precipitated silica. Light scattering (Light), Bonse-Hart USAXS (SAXS-BH), SAXS (SAXS-PH), and WAXS (Diffraction) were used.
- Figure 8 Stress–strain curve of SBR/silica and the corresponding 2D-USAXS images during the deformation process.
- Figure 9 Scattering profiles of SBR/silica swollen by d-hex/h-hex⁶⁹.

Figure 10 Partial scattering function of SBR/silica systems and their fitting results with model functions (solid lines)⁶⁹.

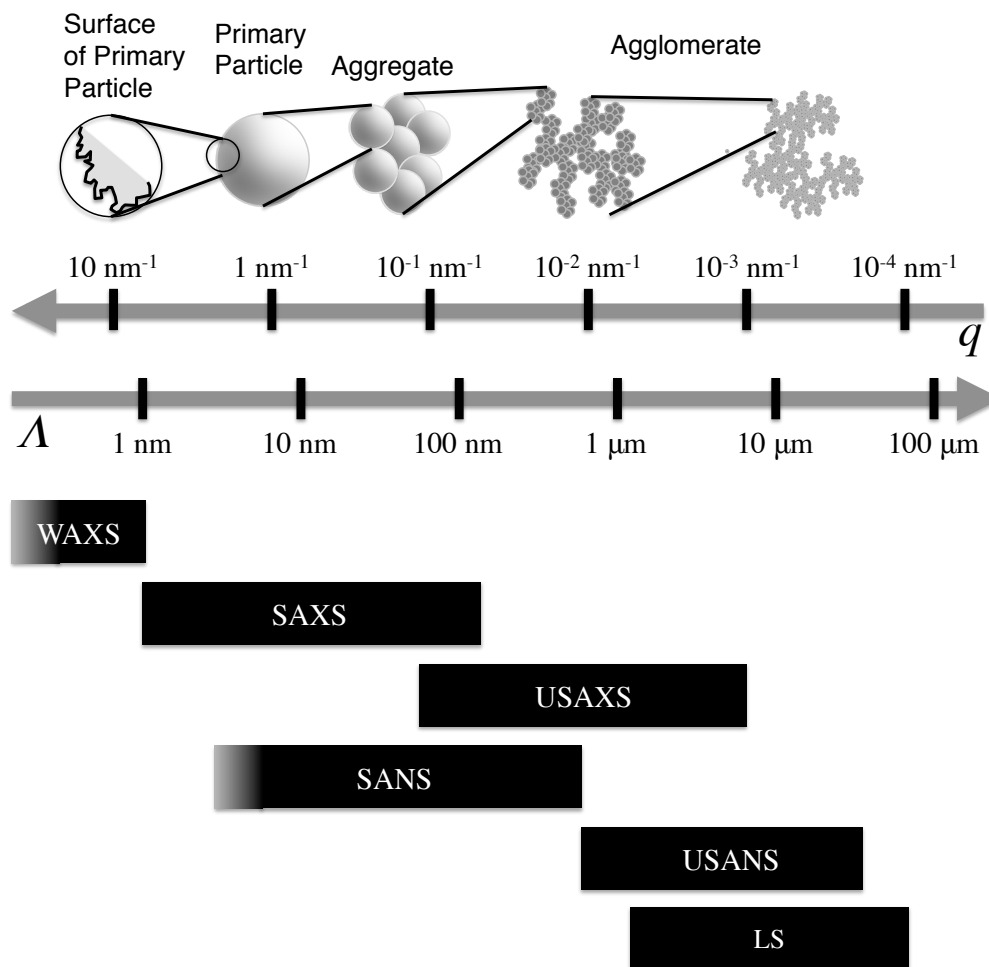


Figure 1

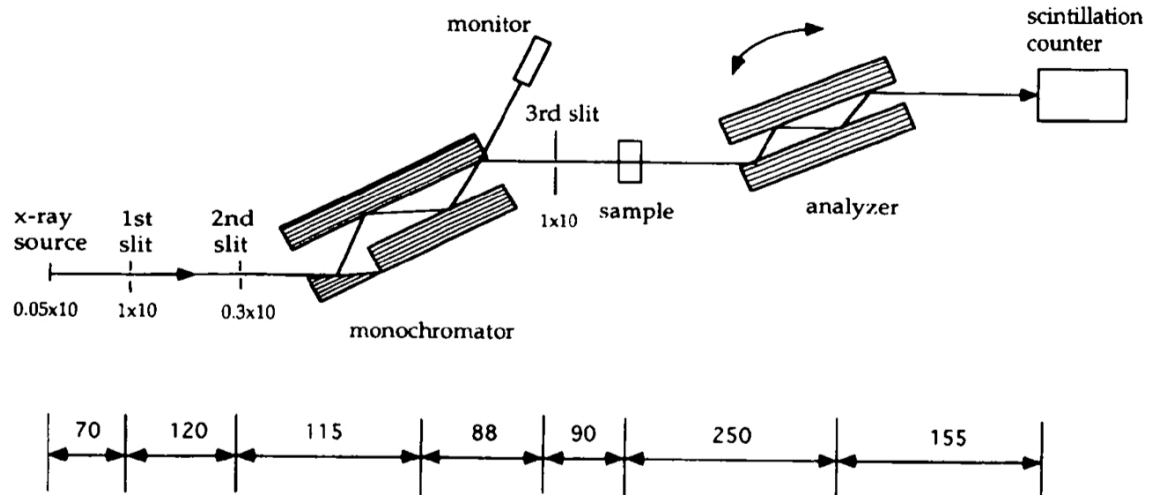


Figure 2

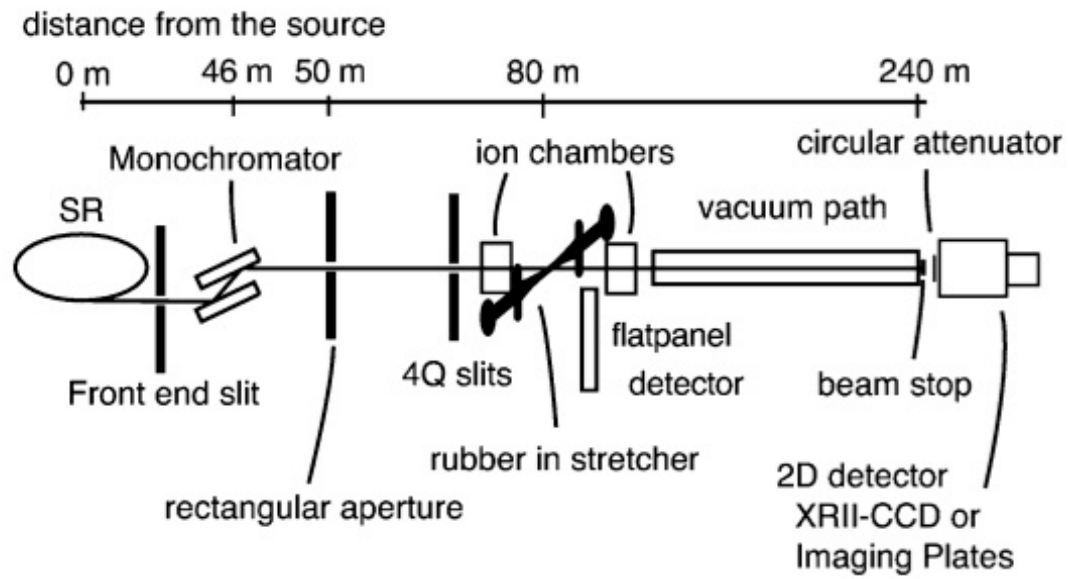


Figure 3

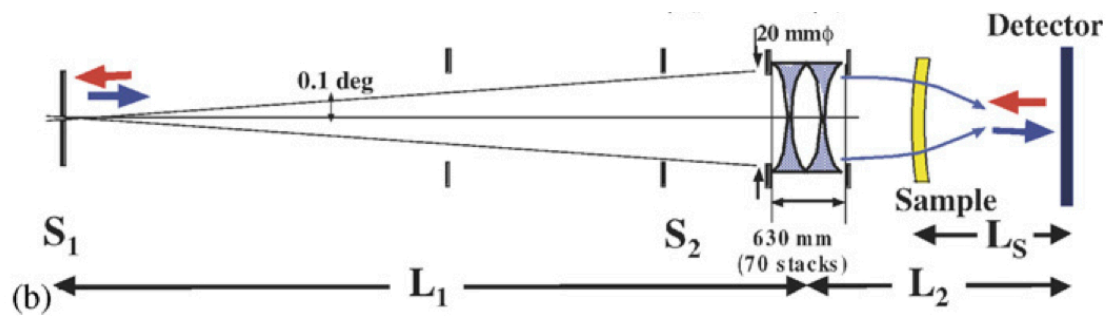


Figure 4

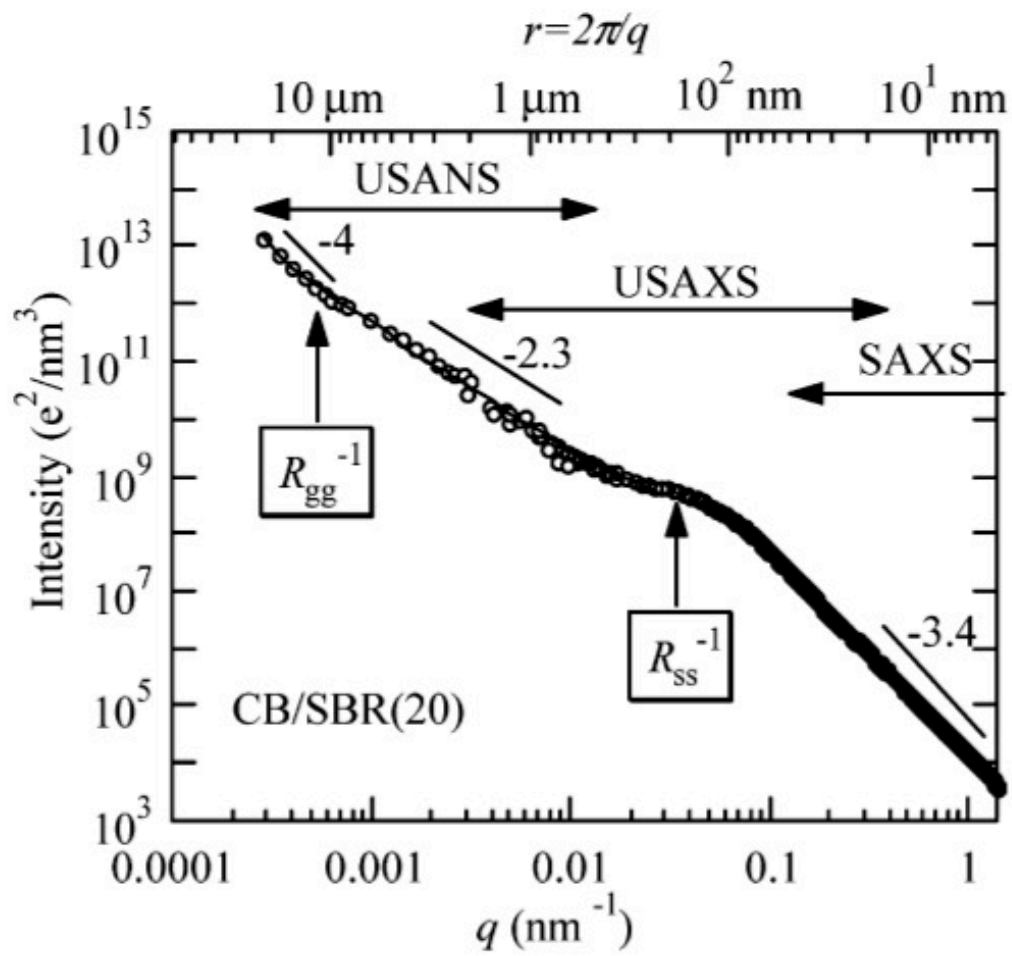


Figure 5

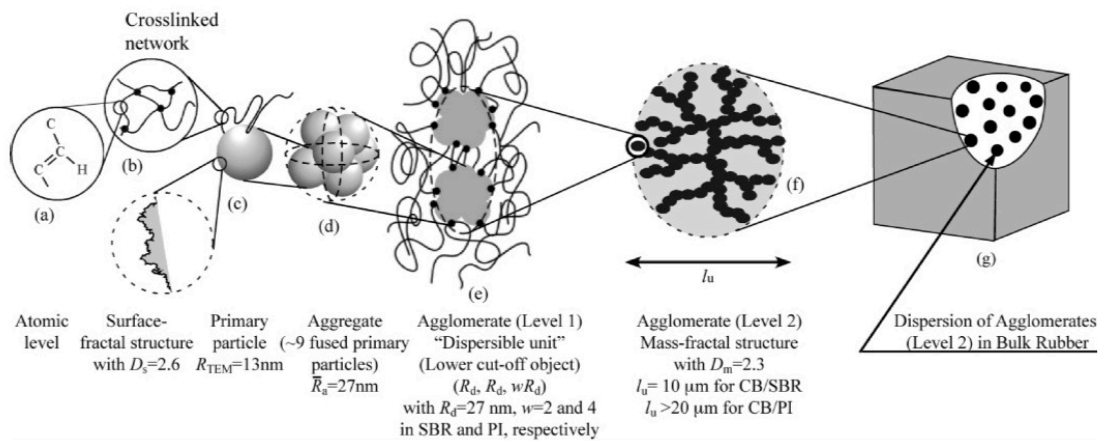


Figure 6

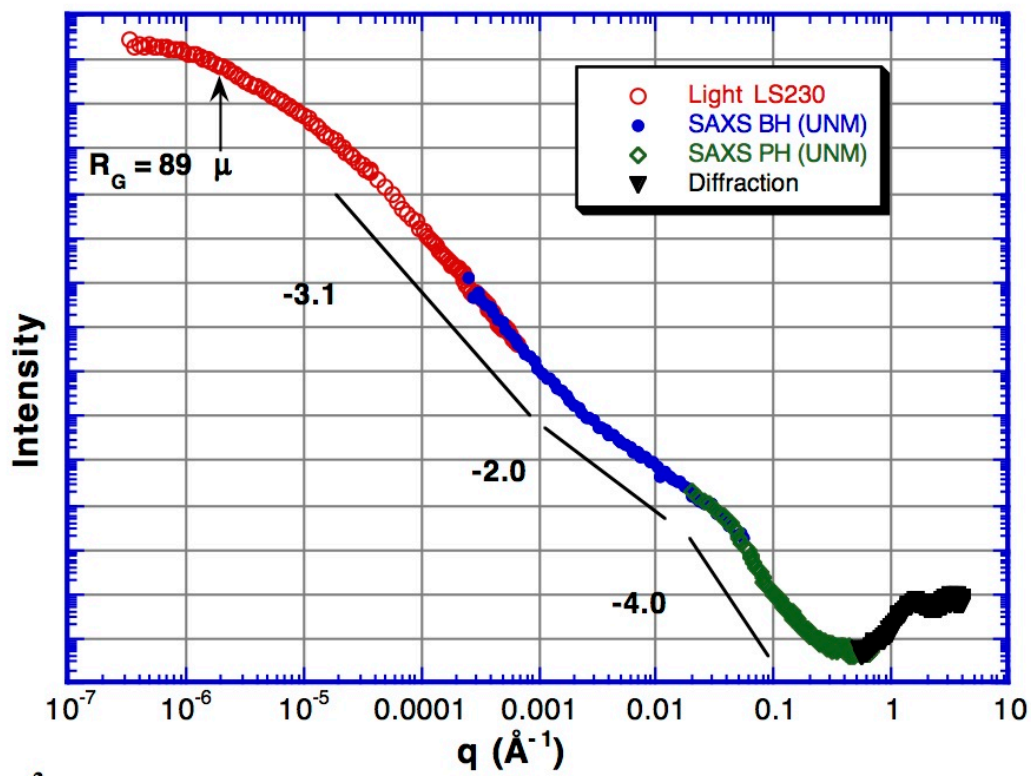


Figure 7

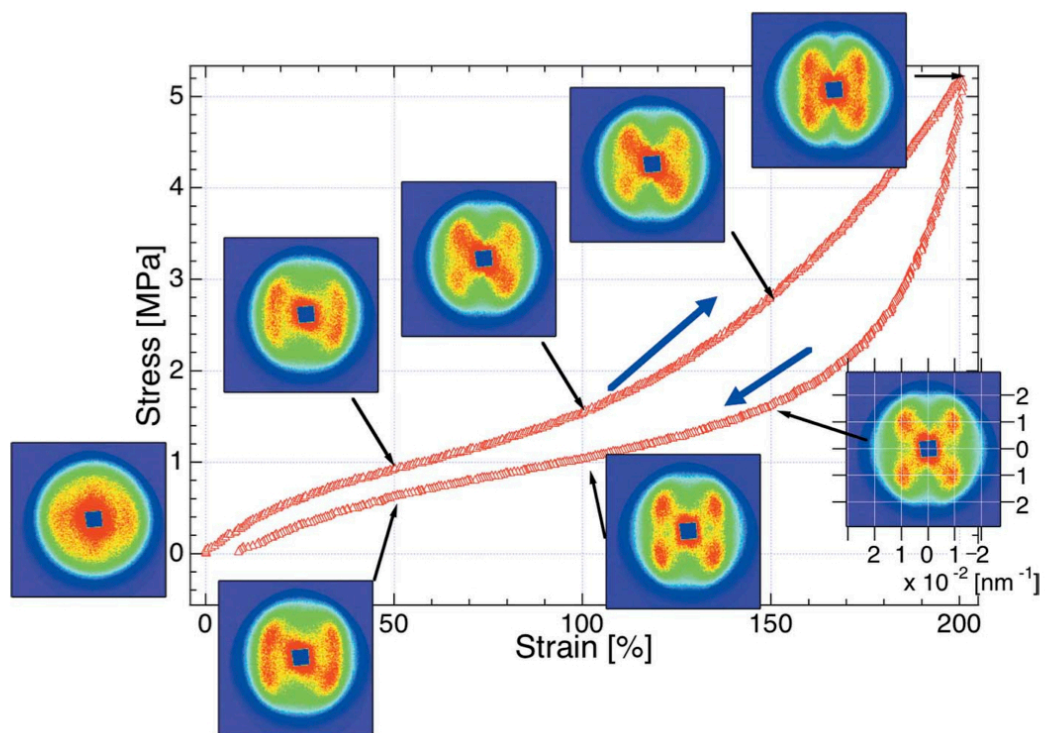


Figure 8

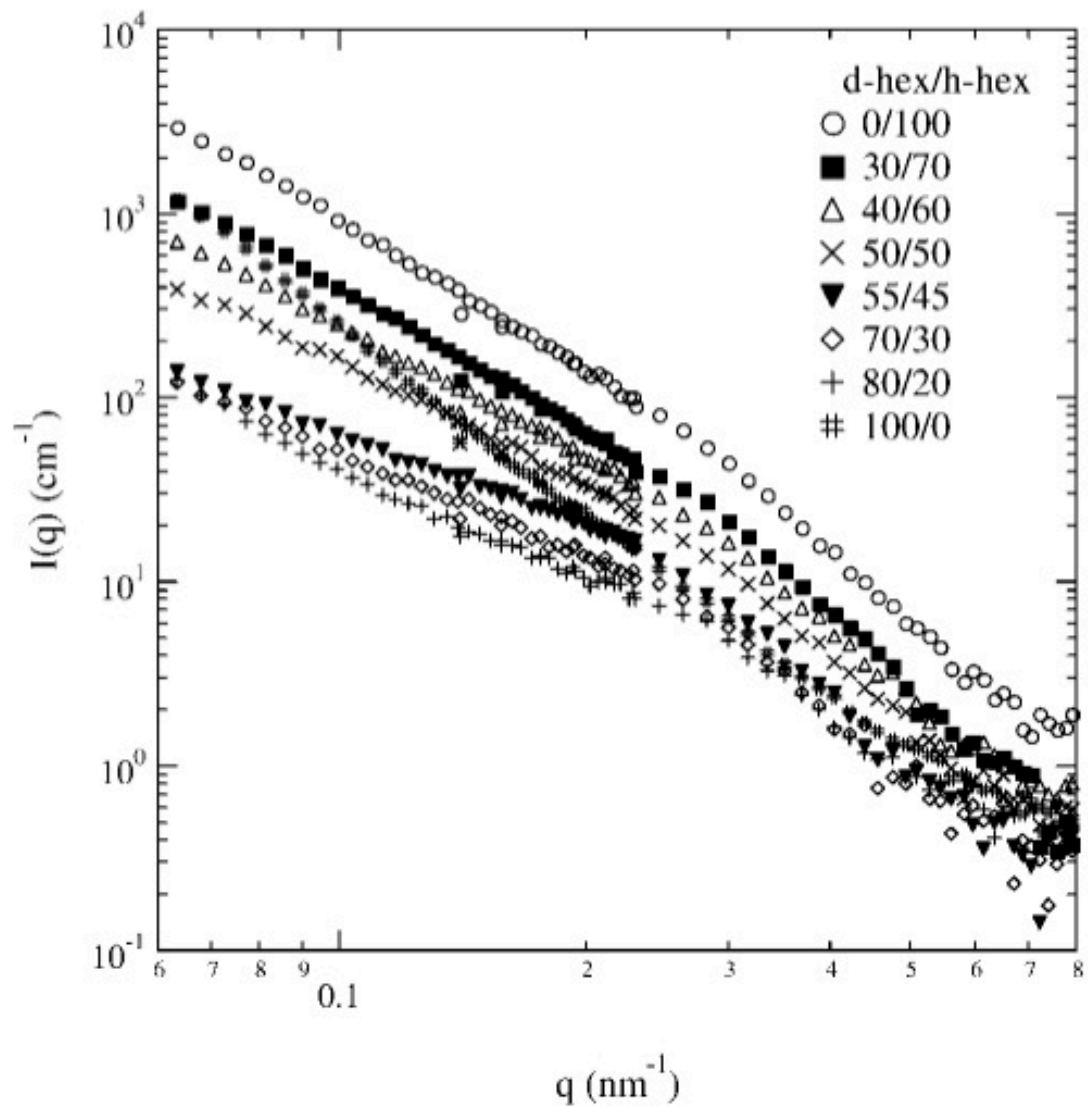


Figure 9

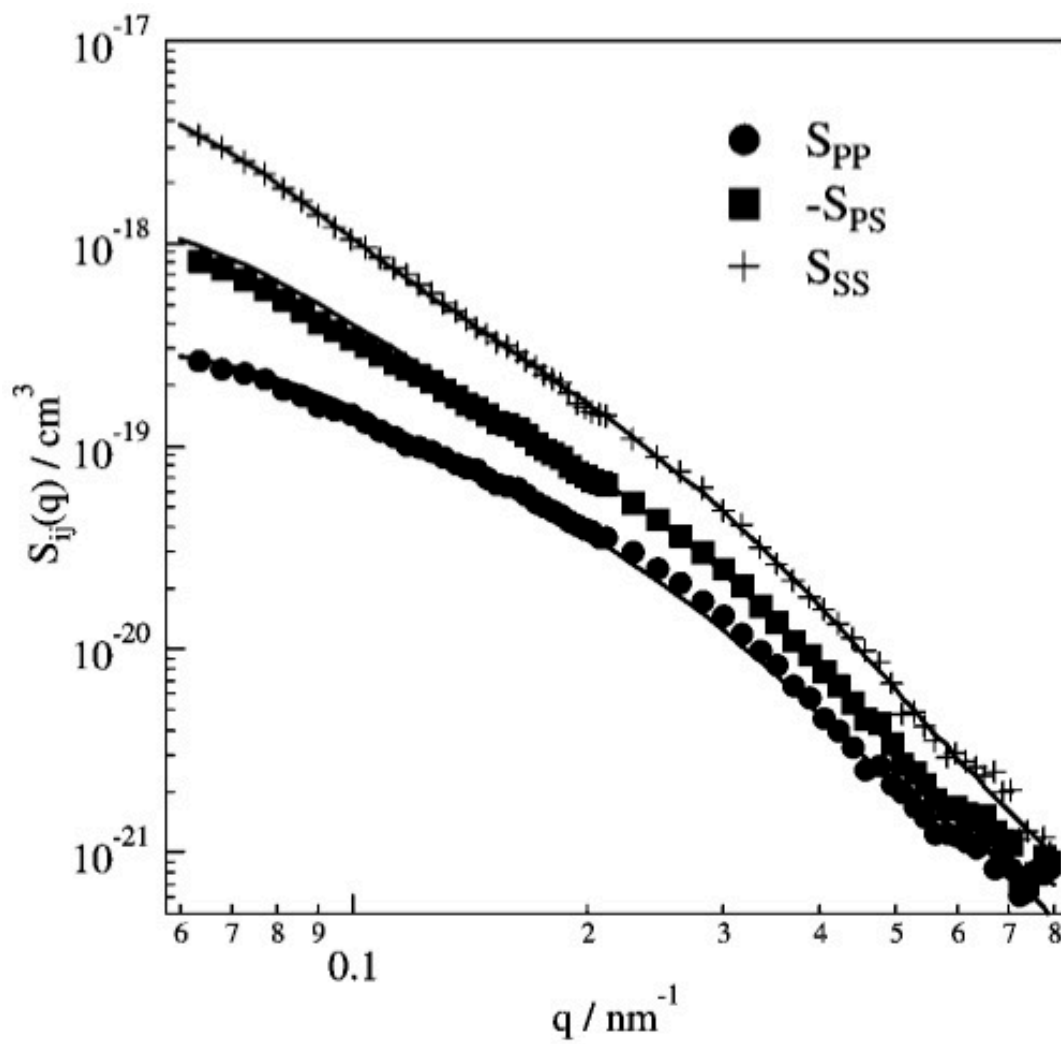


Figure 10